

Hydrostatic pressure effects on the structural and electronic properties of carbon nanotubes

Rodrigo B. Capaz^{1,2,3}, Catalin D. Spataru^{2,3}, Paul Tangney^{2,3}, Marvin L. Cohen^{2,3}, and Steven G. Louie^{2,3}

¹ *Instituto de Física, Universidade Federal do Rio de Janeiro, Caixa Postal 68528, Rio de Janeiro, RJ 21941-972, Brazil*

² *Department of Physics, University of California at Berkeley, Berkeley, CA 94720*

³ *Materials Science Division, Lawrence Berkeley National Laboratory, Berkeley, CA 94720*

Abstract

We study the structural and electronic properties of isolated single-wall carbon nanotubes (SWNTs) under hydrostatic pressure using a combination of theoretical techniques: Continuum elasticity models, classical molecular dynamics simulations, tight-binding electronic structure methods, and first-principles total energy calculations within the density-functional and pseudopotential frameworks. For pressures below a certain critical pressure P_c , the SWNTs' structure remains cylindrical and the Kohn-Sham energy gaps of semiconducting SWNTs have either positive or negative pressure coefficients depending on the value of (n, m) , with a distinct "family" (of the same $n - m$) behavior. The diameter and chirality dependence of the pressure coefficients can be described by a simple analytical expression. At P_c , molecular-dynamics simulations predict that isolated SWNTs undergo a pressure-induced symmetry-breaking transformation from a cylindrical shape to a collapsed geometry. This transition is described by a simple elastic model as arising from the competition between the bond-bending and PV terms in the enthalpy. The good agreement between calculated and experimental values of P_c provides a strong support to the "collapse" interpretation of the experimental transitions in bundles.

PACS numbers: 61.46.+w, 62.25.+g, 73.22.-f

I. INTRODUCTION

Since their discovery [1], carbon nanotubes have been the subject of extensive investigation. Their variable electronic and mechanical properties [2] make them ideal candidates for a variety of applications [3]. Most studies of hydrostatic pressure effects in these materials have focused on the analysis of structural changes in bundles [4, 5, 6, 7, 8, 9, 10, 11, 12, 13, 34]. The interpretation of these changes (ovalization, collapse or polygonization) seems to be obscured by the polydispersity of nanotube diameters in bundles [10, 13]. Therefore, the study of the mechanical response of a single, isolated single-wall carbon nanotube (SWNT) under hydrostatic pressure is of significant value.

Also of great importance is the study of changes in the electronic structure of SWNTs under hydrostatic pressure. Changes in the gap of semiconducting SWNTs upon different types of externally applied deformations have been considered theoretically by many authors [15, 16, 17, 18, 19, 20, 21, 22, 23], but so far the case of hydrostatic pressure has not been addressed. As a special motivation, recent experiments [24] in sodium dodecylsulfate (SDS)-wrapped SWNTs suspended in D₂O show a reduction in the optical gap of all measured SWNTs (with varying diameters and chiralities) upon increasing pressure, a remarkable result that calls for theoretical interpretation.

In this work, we address the changes in structural and electronic properties of semiconducting SWNTs under hydrostatic pressure. Section 2 describes our methodology, consisting of a hierarchy of theoretical techniques, ranging from continuum elasticity models and classical molecular dynamics simulations to tight-binding electronic structure methods and first-principles total energy calculations. In Section 3, structural and electronic properties in the low-pressure regime (below a critical pressure P_c) are presented. In Section 4, the collapse transition at P_c is described. Section 5 lists our main conclusions.

II. METHODOLOGY

Our first-principles calculations are based on density-functional theory (DFT) [25] within the local density approximation (LDA) with the Perdew-Zunger exchange-correlation functional [26]. *Ab initio* Troullier-Martins pseudopotentials [27] are used. Calculations are performed using the SIESTA code [28], which expands the Kohn-Sham wavefunctions in a

linear combination of atomic orbitals (LCAO). A double-zeta plus polarization (DZP) basis is used. The grid cutoff representing the charge density corresponds to a plane-wave energy cutoff of 240 Ry. Isolated nanotubes are modeled by a periodic supercell with sufficiently large lateral dimensions. The irreducible Brillouin Zone is sampled with a 1x1x8 Monkhorst-Pack grid [29]. The effects of hydrostatic pressure P in a SWNT are simulated by imposing a constraint of radially directed external forces with magnitude PA , where A is the surface area per carbon atom. The surface area is calculated by using the *external* radius of the nanotube, i.e. the average nanotube radius plus a van der Waals “exclusion distance” of $\Delta r = 1.675 \text{ \AA}$ (half of the graphite interlayer distance) [5]. The unit cell length along the axis (z direction) is adjusted so that the zz component of the stress tensor (scaled by the ratio between the supercell and nanotube cross-sectional areas) matches the target pressure P . This scheme provides an accurate modeling of structural and electronic properties (within a single-particle description) of an individual carbon nanotube under hydrostatic pressure at $T = 0 \text{ K}$. We apply it to several zig-zag SWNTs in the 5.5 \AA to 15 \AA diameter range.

First-principles calculations are more time-consuming for chiral tubes. However, structural properties are not strongly dependent on chirality. Therefore one can combine the elastic constants calculated within first-principles for zig-zag tubes with an empirical tight-binding (TB) model to calculate the electronic properties of chiral tubes. Although less reliable, the TB calculations are very useful for studying chirality trends since they are computationally less demanding. We use an orthogonal basis of one p orbital per carbon atom, with nearest-neighbor hopping matrix element $\gamma = -2.89 \text{ eV}$ for undistorted bonds [30]. Under hydrostatic pressure, bond components along axial and circumferential directions are distorted according to the radial and axial elastic constants obtained from first-principles. Hopping matrix elements of distorted bonds are modified according to Harrison’s inverse-square rule [31].

Molecular dynamics (MD) simulations allow for the treatment of finite-temperature effects and for a more realistic description of hydrostatic pressure by adding a pressure-transmitting medium. However, they are limited in accuracy owing to the use of classical interatomic potentials. We use a relatively well-tested and reliable potential, namely the extended Tersoff-Brenner potential [32] to model the carbon-carbon bonding of the nanotubes. Hydrostatic pressure is applied to the nanotube using a method similar to that of Martonak *et al.*[33]: The nanotube is immersed in a highly diffusive medium of particles interacting

via a repulsive $1/r^{12}$ potential. The pressure during each simulation is calculated in a box within the full simulation cell which contains only the pressure medium by computing the contributions to the stress tensor from the internal and thermal energies on the particles within this box. This procedure allows hydrostaticity to be easily monitored and alerts one to any problems which may arise from e.g. crystallization or vitrification of the medium.

III. LOW-PRESSURE REGIME

A. Structural properties

For low enough pressures (below P_c), SWNTs remain cylindrical in shape. Therefore, structural changes under pressure are simply described by radial and axial strains, ϵ_r and ϵ_z , respectively. These strains are related to P by radial and axial elastic constants, C_r and C_z [34], defined as $C_r = -P/\epsilon_r$ and $C_z = -P/\epsilon_z$. Fig. 1 shows C_r (squares) and C_z (circles) calculated by first-principles as a function of d for a few zig-zag tubes: (7,0), (8,0), (10,0), (11,0), (14,0), (16,0) and (19,0). As expected for a highly anisotropic material, C_r and C_z are not equal. The same trend was obtained in first-principle calculations in bundles [34]. Moreover, notice the strong diameter dependence of both elastic constants. This dependence can be modeled by treating the nanotube as an elastic sheet with compliance constants S_{11} and S_{12} . By using the standard definitions of Young's modulus $Y = 1/S_{11}$ and Poisson's ratio $\nu = -S_{12}/S_{11}$, and applying geometrical considerations, we arrive at the following expressions [35]:

$$C_r = \frac{4Yr\Delta r}{R_o(2r - \nu R_o)} \quad (1)$$

$$C_z = \frac{4Yr\Delta r}{R_o(R_o - 2\nu r)}, \quad (2)$$

where R_o is the nanotube external radius, $R_o = r + \Delta r$. Best fits give the parameters $Y = 1010$ GPa and $\nu = 0.242$ [36]. The agreement between the first-principles results and the elastic model is remarkable, even for small-diameter tubes.

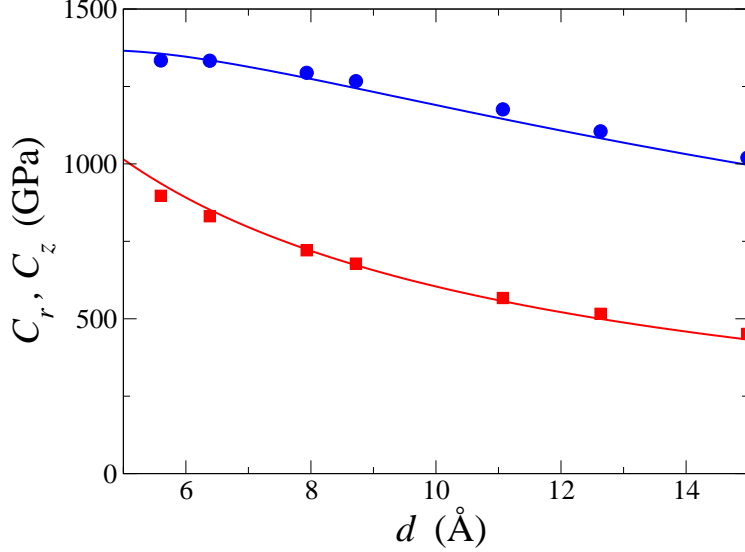


FIG. 1: Elastic constants C_r (red squares) and C_z (blue circles). Lines are best fits using expressions (1) and (2).

B. Electronic properties

Table I shows the calculated pressure coefficients of the LDA band gap, dE_g/dP , for several zig-zag SWNTs. The data reveal two interesting features: (i) The sign of dE_g/dP depends on $q = (n - m) \bmod 3$, being negative for $q = 2$ and positive for $q = 1$; (ii) The magnitude of dE_g/dP seems to increase with diameter. Also shown in Table I are the values of dE_g/dP calculated within TB for the same tubes, so as to compare the accuracy of the TB model for this quantity. The overall agreement is fairly good. The simplicity of the TB model allows us to use it on a wide range of diameters and chiralities. The results are shown in Fig. 2(a). Each dot corresponds to a particular nanotube, and the calculated dE_g/dP are plotted as a function of E_g itself. A more complete picture emerges: Values of dE_g/dP seem to follow trends according to the specific values of $(n - m)$, a so-called “family behavior”. As a guide to the eye, results for nanotubes in the same $(n - m)$ family are grouped by color. The q -dependent sign oscillation found for zig-zag tubes within LDA is a manifestation of this family behavior.

TABLE I: Pressure coefficients for LDA and TB gaps of a few zig-zag SWNTs.

(n, m)	$(dE_g/dP)_{LDA}$	$(dE_g/dP)_{TB}$
	(meV/kbar)	(meV/kbar)
(7,0)	0.63	0.56
(8,0)	-0.17	-0.08
(10,0)	0.80	0.77
(11,0)	-0.40	-0.34
(14,0)	-0.60	-0.57
(16,0)	1.10	1.17
(19,0)	1.20	1.36

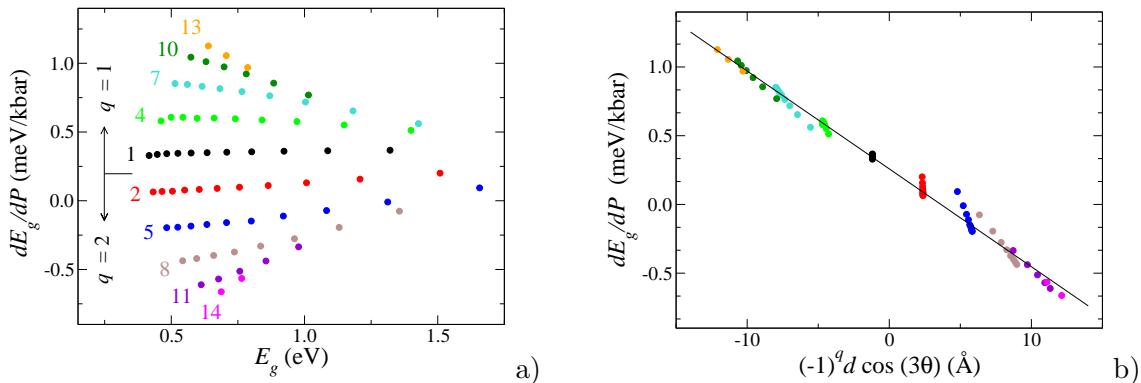


FIG. 2: a) Band-gap pressure coefficient as a function of the gap for a large number of semiconducting SWNTs. Tubes are grouped into colors according to their $(n - m)$ family. The values of $(n - m)$ for each family are also shown in the figure. b) Collapse of dE_g/dP values to a single line when plotted against $(-1)^q d \cos(3\theta)$, using the same color scheme as in Fig.2(a).

Similar types of family behaviors have been found, for instance, in the study of band-gap changes in SWNTs under uniaxial stress [18, 20, 23]. In fact, the two situations (uniaxial stress and hydrostatic pressure) are conceptually identical, differing only in the signs and

magnitudes of the resulting radial and axial strains. Therefore, one can readily adapt the relation for the gap shift from Gartstein *et al.* [23] to the case of hydrostatic pressure:

$$\delta E_g = -\frac{4|\gamma|a_{C-C}}{d}\epsilon_r + 3|\gamma|(\epsilon_r - \epsilon_z)(-1)^q \cos(3\theta), \quad (3)$$

where a_{C-C} is the C-C bond length and θ is the chiral angle. The pressure coefficient then becomes:

$$\frac{dE_g}{dP} = \frac{4|\gamma|a_{C-C}}{C_r d} - 3|\gamma| \left(\frac{1}{C_r} - \frac{1}{C_z} \right) (-1)^q \cos(3\theta). \quad (4)$$

One can obtain a simpler and more useful (albeit approximate) expression by taking the large-diameter limit in the expressions for C_r and C_z . In this limit, both elastic constants decay as $1/d$, and the resulting pressure coefficient is:

$$\frac{dE_g}{dP} = \frac{|\gamma|}{2Y\Delta r} \left[a_{C-C}(2 - \nu) - \frac{3}{4}(1 + \nu)(-1)^q d \cos(3\theta) \right]. \quad (5)$$

We test this analytical expression against our numerical results by plotting dE_g/dP as a function of $(-1)^q d \cos(3\theta)$ in Fig.2(b). The data collapse into a straight line is excellent.

Equation (5) has a very clear physical meaning. Hydrostatic pressure causes an overall shortening of C-C bonds, therefore increasing, in a TB picture, the magnitude of hopping matrix elements. In a graphene sheet, this would lead to an increase in the Fermi velocity. Because, in a simplified picture, energy gaps of semiconducting SWNTs are obtained by slicing the graphene bands, this would lead to an overall tendency of E_g to increase upon applying pressure, for all SWNTs. This is the meaning of the first term in Eq.(5), a chirality-independent positive constant. In addition to that, hydrostatic pressure breaks the triangular lattice symmetry of the parent graphene sheet due to the difference in radial and axial strains. This leads to a relative shift of the slicing planes with respect to the graphene Fermi point. This shift depends on chirality: For $q = 1$ (2), the planes move away from (closer to) the Fermi point, therefore increasing (decreasing) the gap [20]. That is the meaning of the second, chirality-dependent term in Eq. (5).

Experimentally, however, optical gaps of SDS-wrapped SWNTs in aqueous solution show an overall *decrease* with pressure, with magnitudes of dE_g/dP almost ten times higher than our calculated values for similar diameters [24]. A family behavior different from the one described in Eq.(5) is found. Although excitonic effects (not included here) are crucial for a quantitative description of such optical experiments [37], trends are often well described

by a single-particle picture. Therefore, this *qualitative* disagreement between theory and experiment is puzzling and it should motivate further work. It is possible that the interaction between the SDS micelles and the SWNTs plays an important role. Very recent experiments [38] in which strain is applied to SWNTs by both differential thermal contraction upon freezing the D₂O solution and by hydration of a wrapping polymer provide good qualitative agreement (positive and negative shifts depending on chirality) with our theoretical predictions.

IV. THE COLLAPSE TRANSITION

Several high-pressure experiments in bundles indicate some sort of symmetry-breaking phase transition at critical pressures ranging from 1.5 to 2.1 GPa for laser-grown tubes ($d \sim 12 - 14 \text{ \AA}$) [5, 6, 11] and at 6.6 GPa for HiPCo tubes ($d \sim 8 \text{ \AA}$) [13]. One may ask the question: Are those symmetry-breaking transitions induced by bundling or are they related to an intrinsic property of the nanotubes? To investigate how *isolated* SWNTs respond to pressure, MD simulations are performed as described in Section 2. Figs. 3(a) and 3(b) show snapshots of room-temperature simulations at 3 GPa and 4 GPa, respectively, for of a chiral (8,7) SWNT ($d = 10.3 \text{ \AA}$). At 3 GPa, the tube is cylindrical, and at 4 GPa it is collapsed into a flat shape. Therefore, isolated nanotubes indeed suffer a symmetry-breaking transition under hydrostatic pressures. Similar conclusions have been reached by molecular mechanics [39] and elastic models [40]. In fact, Zang *et al.* [40] suggested that a continuous change of cross-section shape (from circular to oval to “peanut” or collapsed) occurs upon increasing pressure beyond P_c . We do not observe any stable oval shape in our MD simulations.

We also formulate a continuum elasticity model to investigate the diameter dependence of the critical pressure P_c . The total enthalpy *per unit length* of the nanotube is written as:

$$h = \frac{\alpha}{2C_0}(C - C_0)^2 + \oint_C ds \frac{\beta}{R^2} + P\mathcal{A}, \quad (6)$$

where C is the perimeter around the tube, C_0 is its value at $P = 0$, R is the local curvature radius and \mathcal{A} is the nanotube cross-sectional area (including the contribution from the van der Waals radius Δr). The first and second terms are continuum versions of the bond-stretching and bond-bending energies, respectively. The parameter α is estimated from the elasticity of graphite: $\alpha = C_{11}c/2 = 3350 \text{ GPa}\cdot\text{\AA}$, where $c/2$ is the interplanar distance of

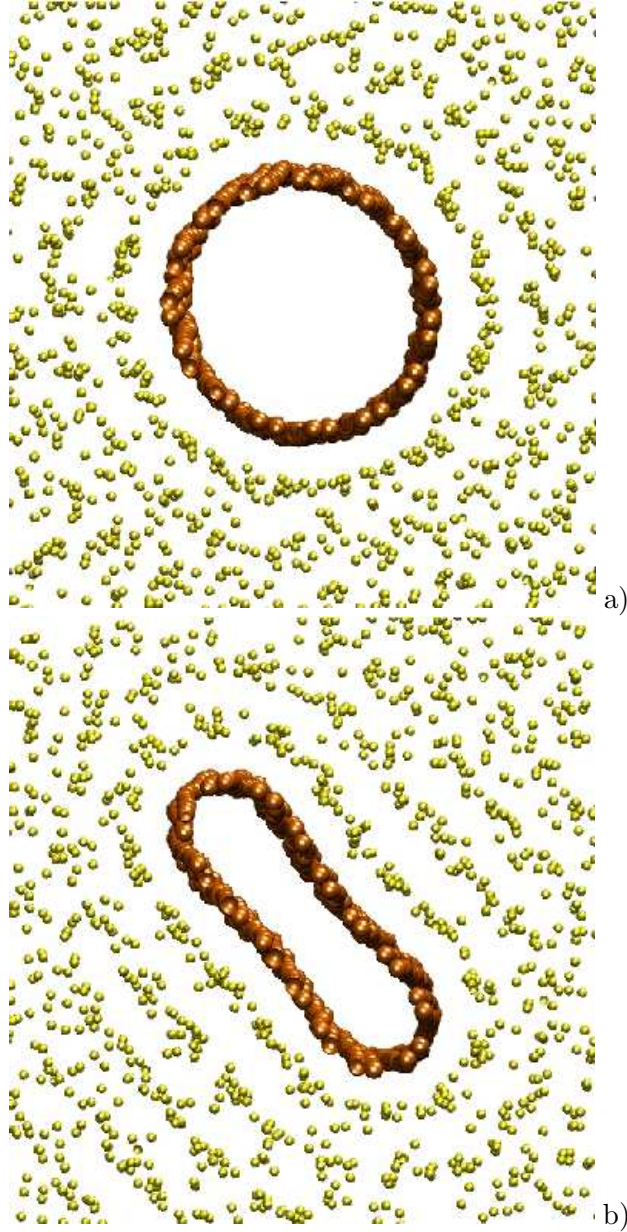


FIG. 3: Snapshots of room-temperature MD simulations of a (8,7) SWNT at (a) 3 GPa and (b) 4GPa. Large orange balls and small yellow balls represent carbon atoms in the nanotube and repulsive Lennard-Jones medium particles, respectively.

graphite. The parameter β is extracted from first-principles calculations of strain energy of nanotubes with varying diameters [41], yielding $\beta = 133 \text{ GPa}\cdot\text{\AA}^3$. The onset of instability of the cylindrical shape is searched by monitoring the change in enthalpy δh when a small circular-to-elliptical deformation is applied to the cross-section, at different pressures. For $P > P_c$, δh should be negative. This procedure is convenient since it allows the use of the

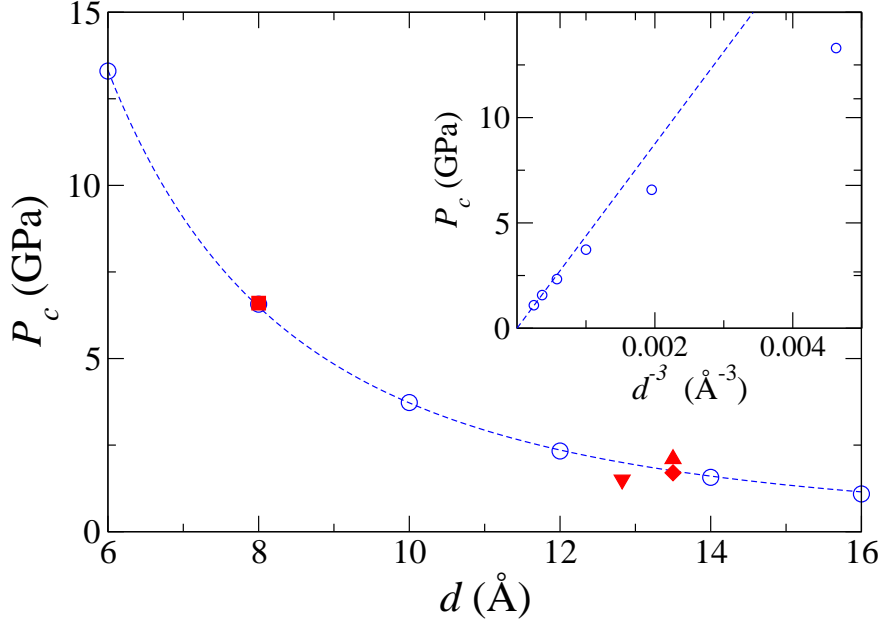


FIG. 4: Critical pressure for collapsing as a function of nanotube diameter. Open blue dots are the elastic-model calculated results, the blue dashed line is a guide to the eye. Full red symbols are experimental results. Square: Ref. [13], up-triangle: Ref. [11], down-triangle: Ref. [5], diamond: Ref. [6]. In the inset, P_c is plotted against $1/d^3$. The straight line represents the limiting $1/d^3$ behavior.

well-known formulae for the ellipse perimeter, area and curvature radius. In accordance with Ref. [40], we find that instability is driven by the competition between the bond-bending energy (that tends to keep the circular cross-section) and the PV term (that tends to decrease the nanotube volume by collapsing it).

Figure 4 shows the calculated values of P_c as a function of nanotube diameter. As one can see, P_c decreases with increasing diameter, as suggested in recent theoretical works [13, 39, 40]. In the inset of Fig. 4, we confirm that P_c decays as $1/d^3$ in the limit of large tubes, in agreement with the classic study by Lévy on the theory of elastic rings [42]. Also shown in the figure are the available experimental data. The agreement is excellent, indicating that the instability of individual tubes under pressure is most likely the driving force for the observed phase transitions in bundles.

V. CONCLUSIONS

We have investigated the structural and electronic properties of semiconducting SWNTs under hydrostatic pressure. For low enough pressures, nanotubes remain cylindrical and are described by radial and axial strains. Radial strains are larger than axial strains, a result that is well described by the elastic properties of a graphene sheet. Pressure coefficients for the single-particle band gap can be positive or negative, with strong family behavior, in disagreement with recent optical measurements in micelle-wrapped tubes in aqueous solution [24]. At a certain critical pressure P_c , isolated SWNTs collapse from cylindrical to a flat shape. The good agreement between calculated and experimental critical pressures indicate that such a pressure-induced instability of isolated SWNTs is the driving force for the observed transitions in bundles.

We acknowledge useful discussions with J. Wu. RBC acknowledges financial support from the John Simon Guggenheim Memorial Foundation and Brazilian funding agencies CNPq, FAPERJ, Instituto de Nanociências, FUJB-UFRJ and PRONEX-MCT. Work partially supported by NSF Grant No. DMR00-87088 and DOE Contract No. DE-AC03-76SF00098. Computer time was provided by the NSF at the National Center for Supercomputing Applications and by the DOE at the Lawrence Berkeley National Laboratory (LBNL)'s NERSC center.

-
- [1] S. Iijima, *Nature (London)* **354**, 56 (1991).
 - [2] M. S. Dresselhaus, G. Dresselhaus, and P. Avouris (eds.), *Carbon Nanotubes, Topics in Applied Physics*, Vol. 80 (Springer-Verlag, Berlin, 2001).
 - [3] R. H. Baughman, A. A. Zakhidov, and W. A. de Heer, *Science* **297**, 787 (2002).
 - [4] S. A. Chesnokov, V. A. Nalimova, A. G. Rinzler, R. E. Smalley, and J. E. Fischer, *Phys. Rev. Lett.* **82**, 343 (1999).
 - [5] U. D. Venkateswaran, A. M. Rao, E. Richter, M. Menon, A. Rinzler, R. E. Smalley, and P. C. Eklund, *Phys. Rev. B* **59**, 10928 (1999).
 - [6] M. J. Peters, L. E. McNeil, J. P. Lu, and D. Kahn, *Phys. Rev. B* **61**, 5939 (2000).
 - [7] J. Tang, L.-C. Qin, T. Sasaki, M. Yudasaka, A. Matsushita, and S. Iijima, *Phys. Rev. Lett.* **85** 1887 (2000).

- [8] S. M. Sharma, S. Karkamar, S. K. Sikka, P. V. Teredesai, A. K. Sood, A. Govindaraj, and C. N. R. Rao, *Phys. Rev. B* **63**, 205417 (2001).
- [9] S. Rols, I. N. Goncharenko, R. Almairac, J. L. Sauvajol, and I. Mirebeau, *Phys. Rev. B* **64**, 153401 (2001).
- [10] M. H. F. Sluiter, V. Kumar, and Y. Kawazoe, *Phys. Rev. B* **65**, 161402 (2002).
- [11] J. Sandler, M. S. P. Shaffer, A. H. Windle, M. P. Halsall, M. A. Montes-Morán, C. A. Cooper, and R. J. Young, *Phys. Rev. B* **67**, 035417 (2003).
- [12] U. D. Venkateswaran, D. L. Masica, G. U. Sumanasekera, C. A. Furtado, U. J. Kim, and P. C. Eklund, *Phys. Rev. B* **68**, 241406 (2003).
- [13] J. A. Elliott, J. K. W. Sandler, R. J. Young, A. H. Windle, and M. S. P. Shaffer, *Phys. Rev. Lett.* **92**, 095501 (2004).
- [34] S. Reich, C. Thomsen, and P. Ordejón, *phys. stat. sol.(b)* **235**, 354 (2003).
- [15] J. -C. Charlier, Ph. Lambin, and T. W. Ebbesen, *Phys. Rev. B* **54**, R8377 (1996).
- [16] C. L. Kane and E. J. Mele, *Phys. Rev. Lett.* **78**, 1932 (1997).
- [17] R. Heyd, A. Charlier, and E. McRae, *Phys. Rev. B* **55**, 6820 (1997).
- [18] L. Yang, M. P. Anantram, J. Han, and J. P. Lu, *Phys. Rev. B* **60**, 13874 (1999).
- [19] P. E. Lammert, P. Zhang, and V. H. Crespi, *Phys. Rev. Lett.* **84**, 2453 (2000).
- [20] L. Yang and J. Han, *Phys. Rev. Lett.* **85**, 154 (2000).
- [21] M. S. C. Mazzoni and H. Chacham, *Appl. Phys. Lett.* **76**, 1561 (2000).
- [22] O. Gülseren, T. Yildirim, S. Ciraci, and Ç. Kiliç, *Phys. Rev. B* **65**, 155410 (2002).
- [23] Yu. N. Gartstein, A. A. Zakhidov, and R. H. Baughman, *Phys. Rev. B* **68**, 115415 (2003).
- [24] J. Wu, W. Walukiewicz, W. Shan, E. Bourret-Courchesne, J. W. Ager III, K. M. Yu, E. E. Haller, K. Kissel, S. M. Bachilo, R. B. Weisman, and R. E. Smalley, *Phys. Rev. Lett.*, **93**, 017404 (2004).
- [25] W. Kohn and L. J. Sham, *Phys. Rev.* **140**, A1133 (1965).
- [26] J. P. Perdew and A. Zunger, *Phys. Rev. B* **23**, 5048 (1981).
- [27] N. Troullier and J. L. Martins, *Phys. Rev.* **43**, 1993 (1991).
- [28] P. Ordejón, E. Artacho, and J. M. Soler, *Phys. Rev. B* **53**, R10441 (1996), J. M. Soler, E. Artacho, J. D. Gale, A. García, J. Junquera, P. Ordejón, and D. Sánchez-Portal, *J. Phys.: Condens. Matter* **14**, 2745 (2002).
- [29] H. J. Monkhorst and J. D. Pack, *Phys. Rev. B* **13**, 5188 (1976).

- [30] A. G. Souza Filho, S. G. Chou, Ge. G. Samsonidze, G. Dresselhaus, M. S. Dresselhaus, L. An, J. Liu, A. K. Swan, M. S. Ünlü, B. B. Goldberg, A. Jorio, A. Grüneis, and R. Saito, *Phys. Rev. B* **69**, 115428 (2004).
- [31] W. A. Harrison, *Electronic Structure and the Properties of Solids* (Dover, New York, 1989).
- [32] D. W. Brenner, O. A. Shenderova, J. A. Harrison, S. J. Stuart, B. Ni, and S. B. Sinnott, *J. Phys.: Condens. Matter* **14**, 783 (2002).
- [33] R. Martonak, C. Molteni, and M. Parrinello, *Phys. Rev. Lett.* **84**, 682 (2000).
- [34] S. Reich, C. Thomsen, and P. Ordejón, *Phys. Rev. B* **65**, 153407 (2002).
- [35] R. B. Capaz, C. Spataru, P. Tangney, M. L. Cohen, and S. G. Louie, to be published.
- [36] These parameters should not be interpreted as the Young's modulus and Poisson's ratio of nanotubes, although their values are close to some of the reported values in the literature for these quantities.
- [37] C. D. Spataru, S. Ismail-Beigi, L. X. Benedict, and S. G. Louie, *Phys. Rev. Lett.* **92**, 077402 (2004).
- [38] L.-J. Li, R. J. Nicholas, R. S. Deacon, and P. A. Shields, *Phys. Rev. Lett.*, to be published.
- [39] C. Li and T.-W. Chou, *Phys. Rev. B* **69**, 073401 (2004).
- [40] J. Zang, A. Treibergs, Y. Han, and F. Liu, *Phys. Rev. Lett.* **92**, 105501 (2004).
- [41] J. W. Mintmire and C. T. White, *Carbon* **33**, 893 (1995).
- [42] M. Lévy, *Journal de Mathématiques Pures et Appliquées*, ser. 3, VII (1884).